

# A bright-rimmed cloud sculpted by the H II region

## Sh2-48

M. E. Ortega<sup>1</sup>, S. Paron<sup>1,2,3</sup>, E. Giacani<sup>1,2</sup>, M. Rubio<sup>4</sup>, and G. Dubner<sup>1</sup>

<sup>1</sup> Instituto de Astronomía y Física del Espacio (IAFE), CC 67, Suc. 28, 1428 Buenos Aires, Argentina

e-mail: mortega@iafe.uba.ar

<sup>2</sup> FADU - Universidad de Buenos Aires, Ciudad Universitaria, Buenos Aires

<sup>3</sup> CBC - Universidad de Buenos Aires, Ciudad Universitaria, Buenos Aires

<sup>4</sup> Departamento de Astronomía, Universidad de Chile, Casilla 36-D, Santiago, Chile

Received <date>; Accepted <date>

### ABSTRACT

**Aims.** To characterize a bright-rimmed cloud embedded in the H II region Sh2-48 searching for evidence of triggered star formation.

**Methods.** We carried out observations towards a region of  $2' \times 2'$  centered at RA=18<sup>h</sup> 22<sup>m</sup> 11.39<sup>s</sup>, dec.=−14° 35' 24.81'' (J2000) using the Atacama Submillimeter Telescope Experiment (ASTE; Chile) in the <sup>12</sup>CO J=3–2, <sup>13</sup>CO J=3–2, HCO<sup>+</sup> J=4–3, and CS J=7–6 lines with an angular resolution of about 22''. We also present radio continuum observations at 5 GHz carried out with the Jansky Very Large Array (JVLA; EEUU) interferometer with a synthesized beam of  $7'' \times 5''$ . The molecular transitions are used to study the distribution and kinematics of the molecular gas of the bright-rimmed cloud. The radio continuum data is used to characterize the ionized gas located at the illuminated border of this molecular condensation. Combining these observations with infrared public data allows us to build up a comprehensive picture of the current state of star formation within this cloud.

**Results.** The analysis of our molecular observations reveals the presence of a relatively dense clump with  $n(\text{H}_2) \sim 3 \times 10^3 \text{ cm}^{-3}$ , located in projection onto the interior of the H II region Sh2-48. The emission distribution of the four observed molecular transitions has, at  $V_{\text{LSR}} \sim 38 \text{ km s}^{-1}$ , morphological anti-correlation with the bright-rimmed cloud as seen in the optical emission. From the new radio continuum observations we identify a thin layer of ionized gas located at the border of the clump which is facing to the ionizing star. The ionized gas has an electron density of about  $73 \text{ cm}^{-3}$  which is a factor three higher than the typical critical density ( $n_c \sim 25 \text{ cm}^{-3}$ ) above which an ionized boundary layer can be formed and be maintained. This fact supports the hypothesis that the clump is being photoionized by the nearby O9.5V star, BD-14 5014. From

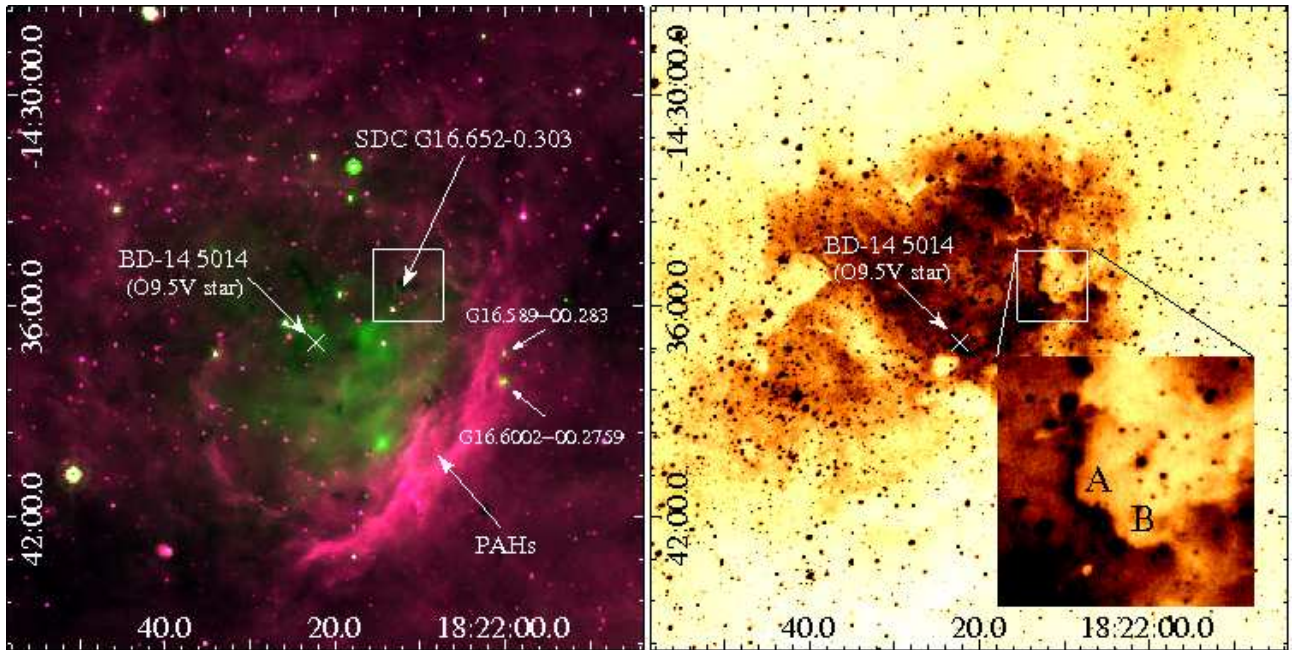


**Fig. 1.** Left) *Spitzer* two-color images (8  $\mu$ m in red and 24  $\mu$ m in green) of the infrared dust bubble N18 (infrared counterpart of Sh2-48). The white box indicates the region mapped with ASTE which includes the BRC. The position of the ionizing star BD-14 5014 is shown. Red and green scales go from 60 to 160 and from 35 to 350 MJy/sr, respectively. Right)  $H\alpha$  image of the H II region Sh2-48 as obtained from the Super COSMOS H-alpha Survey (SHS). A close up view of the BRC is shown where the features A and B are indicated. The scale goes from 2600 (white) to 10000 R (black).

the evaluation of the pressure balance between the ionized and molecular gas, we conclude that the clump would be in a pre-pressure balance state with the shocks being driven into the surface layer. Among the five YSO candidates found in the region, two of them (class I), are placed slightly beyond the bright rim suggesting that their formation could have been triggered via the radiation-driven implosion process.

**Key words.** Stars: formation – ISM: clouds – (ISM): H II regions

## 1. Introduction

Bright-rimmed clouds (BRCs) are small dense clouds located at the border of evolved H II regions. The illumination of these dark clumps by nearby OB stars might be responsible for triggered collapse and subsequent star formation (e.g. Sandford et al. 1982; Bertoldi 1989; Lefloch & Lazareff 1994). The process begins when the ionization front associated with an H II region moves over a pre-existing molecular condensation, creating a dense outer shell of ionized gas named: ionized boundary layer (IBL), which surrounds the rim of the clump. If the IBL is over-pressured with respect to the molecular gas within the BRC, shocks are driven into the cloud compressing the molecular material until the internal pressure is balanced with the pressure of the IBL (about  $10^5$  yr later). At this stage the collapse of the clump begins a process leading to the creation of a new generation of stars. After that, the shock front dissipates and the cloud is considered to be in a quasi-steady state known as the cometary globule stage ( $\sim 10^6$  yr; Bertoldi & McKee 1990;

Lefloch & Lazareff 1994). This mechanism of triggered star formation, known as radiation-driven implosion (RDI), was first proposed by Reipurth (1983), and may be responsible for the production of hundreds of stars in each H II region (Ogura et al. 2002). Finally, the mass loss resulting from photo-evaporative processes ultimately leads to the destruction of the cloud on a timescale of several million years (Megeath & Wilson 1997).

Star formation in BRCs has long been suspected (e.g. Wootten et al. 1983). Sugitani et al. (1991) and Sugitani & Ogura (1994) compiled catalogs (the so-called SFO Catalog) of 44 BRCs in the northern sky and 45 BRCs in the southern sky, each associated with an IRAS point source of low dust temperature. Near-IR imaging observations by Sugitani et al. (1995) indicated that BRCs are often associated with a small cluster of young stars showing not only an asymmetric spatial distribution with respect to the cloud but also a possible age gradient. Sugitani et al. (2000) report that young stellar objects (YSOs) detected inside BRCs tend to lie close to the line joining the center of mass of the cloud and the ionizing stars. Detailed characterization of the physical properties of some BRCs included in the SFO Catalog were made based on submillimeter and radio continuum observations (e.g. Morgan et al. 2004; Thompson et al. 2004; Urquhart et al. 2006; Morgan et al. 2008 and references therein). Some authors concluded that a radiative-driven implosion mechanism is in progress in many (but not all) of the SFO BRCs and that massive stars are being formed there (Urquhart et al. 2009).

In this work, we present new molecular line data towards a BRC associated with the H II region Sh2-48, obtained using the Atacama Submillimeter Telescope Experiment (ASTE) and radio continuum observations at 5 GHz carried out using the Jansky Very Large Array (JVLA). We characterize the molecular clump and its associated IBL, and investigate the balance pressure between the molecular and the ionized gas using our observations which, when combined with public infrared (IR) data, provide a comprehensive picture of the star formation process associated with this BRC and allow us to discern whether or not it was triggered by the proposed mechanism.

### 1.1. Presentation of a BRC embedded in the H II region Sh2-48

Sh2-48 is an irregular H II region about 10' in size, centered at RA = 18<sup>h</sup>22<sup>m</sup>24.1<sup>s</sup>, dec. = -14°35'09'' (J2000) which was first catalogued by Sharpless (1959). Avedisova & Kondratenko (1984) identified the star BD-14 5014 with spectral type O9.5V (Vogt & Moffat 1975; Vijapurkar & Drilling 1993) as the exciting star of Sh2-48. Lockman (1989), based on radio recombination lines, estimated for Sh2-48 a radial velocity of  $\sim 44.9 \text{ km s}^{-1}$ , while Blitz et al. (1982) in their Catalog of CO radial velocities toward Galactic H II regions reported a molecular cloud related to Sh2-48 at  $44.6 \text{ km s}^{-1}$ . Later, Anderson et al. (2009) detected molecular gas associated with the H II region at a radial velocity of about  $43.2 \text{ km s}^{-1}$ , which using a flat rotation model for our Galaxy (with  $R_{\odot} = 7.6 \pm 0.3 \text{ kpc}$  and  $\Theta_{\odot} = 214 \pm 7 \text{ km s}^{-1}$ ) corresponds to the near and far distances of about 3.8 and 12.4 kpc, respectively. Based on H I absorption studies, the authors resolved the ambiguity in favor of the far distance. However, several works based on spectrophotometry studies of

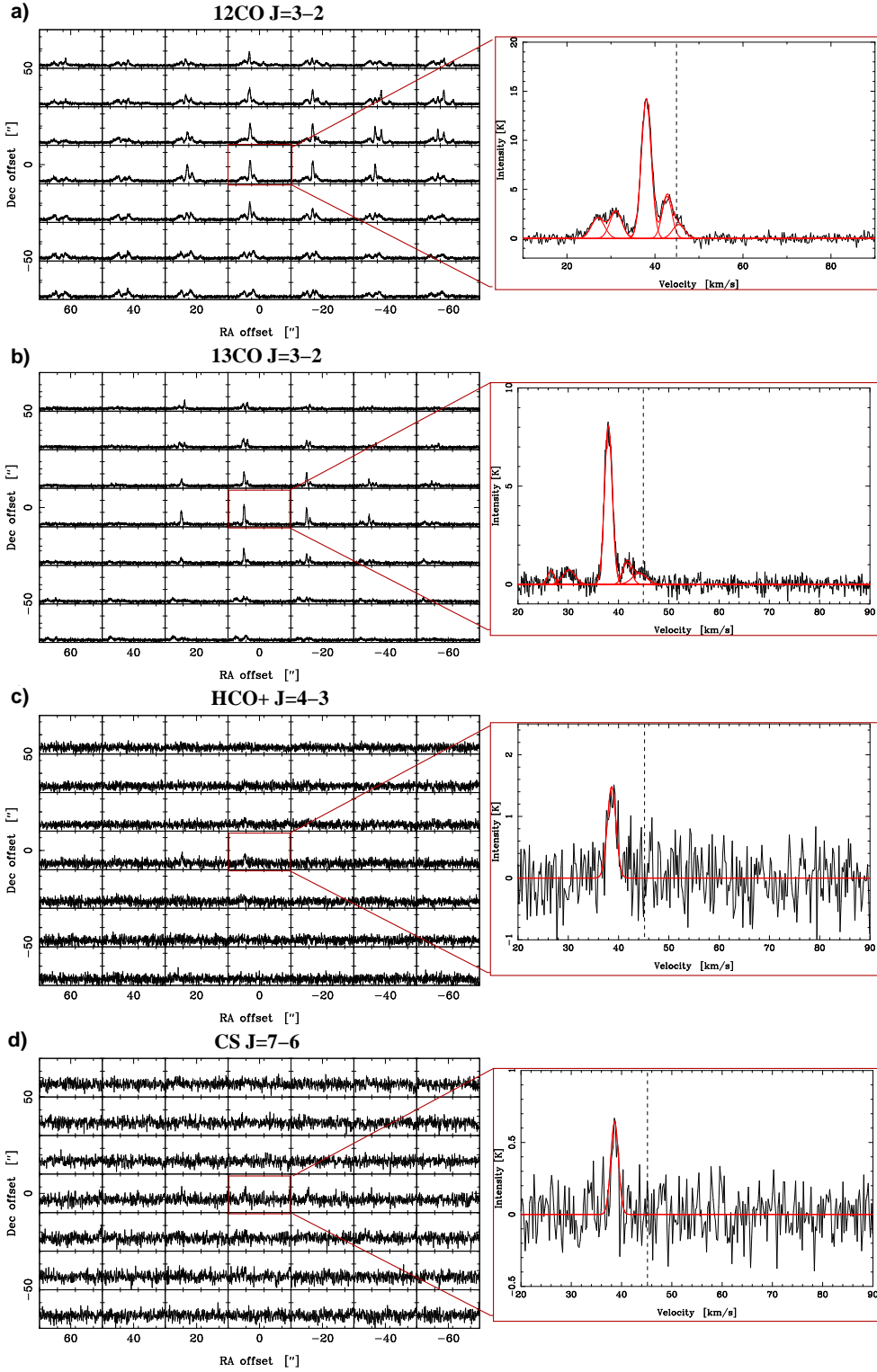


**Fig. 2.** Left-column:  $^{12}\text{CO J=3-2}$  (a),  $^{13}\text{CO J=3-2}$  (b),  $\text{HCO}^+ \text{ J=4-3}$  (c), and  $\text{CS J=7-6}$  (d) spectra obtained towards the  $2' \times 2'$  region (white box in Fig. 1) mapped with ASTE. Right-column: spectra towards the position (0, 0) of the four transitions smoothed to a velocity resolution of  $0.22 \text{ km s}^{-1}$ . The single or multiple-component Gaussian fits are shown in red. The dashed line marks the systemic velocity of the molecular cloud. All velocities are in local standard of rest.

BD-14 5014 (e.g. Vogt & Moffat 1975; Crampton et al. 1978; Avedisova & Kondratenko 1984) established better constraints in favor of the near distance for the ionizing star of Sh2-48. In what follows we adopt 3.8 kpc as the most likely distance to Sh2-48 and its associated BRC.

The Infrared Dust Bubbles Catalog compiled by Churchwell et al. (2006), includes the bubble N18, which can be identified as the H II region Sh2-48 with its associated photodissociation region (PDR; seen at  $8\ \mu\text{m}$ ). In Figure 1-left we present a composite two-color image ( $8\ \mu\text{m}$  in red and  $24\ \mu\text{m}$  in green) of N18. N18 is an open infrared dust bubble with spiraling filaments at  $8\ \mu\text{m}$  that partially encircle the emission at  $24\ \mu\text{m}$ , mainly related to the small dust grains. On the western border of the bubble, Deharveng et al. (2010) identified two compact radio sources with associated  $24\ \mu\text{m}$  emission, G16.6002–00.2759 and G16.589–00.283, suggesting that they are likely compact H II regions whose association with N18 is uncertain. In this paper, we focus our attention in a particularly interesting region (delimited in Fig. 1 with a white box) where we identify a new BRC. This BRC has not any IRAS point source associated, and has not been included in the SFO Catalog. As seen in projection, it appears to be embedded within Sh2-48 towards the northwestern border of the H II region. The associated bright rim, better appreciated at  $8\ \mu\text{m}$ , delineates the border of the catalogued *Spitzer* dark cloud SDC G16.652-0.303 which is facing the ionizing star. The curved morphology of the illuminated bright rim suggests that the action of the nearby O star must have shaped the dark molecular cloud.

Figure 1-right shows an image of the  $H_\alpha$  emission arising from the ionized gas associated with Sh2-48 as obtained from the Super COSMOS H-alpha Survey (SHS). The optical image highlights the illuminated border of the BRC (see white box). The bright rim is clearly facing the ionizing star and preceding a region of high visual extinction associated with the above mentioned *Spitzer* dark cloud SDC G16.652-0.303. The ionized gas appears to be located onto the surface of the BRC. A close up view of the BRC included in Fig. 1-right, shows two curved features, labeled A and B, which may have been sculpted by the action of the H II region. In particular, the bright rim associated with the feature A is the brightest one, which is in agreement with the fact that it is the only one detected at  $8\ \mu\text{m}$ .

## 2. Observations and data reduction

### 2.1. Molecular observations

The molecular line observations were carried out on June 12 and 13, 2011 with the 10m Atacama Submillimeter Telescope Experiment (ASTE; Ezawa et al. 2004). We used the CATS345 GHz band receiver, which is a two-single band SIS receiver remotely tunable in the LO frequency range of 324-372 GHz. We simultaneously observed  $^{12}\text{CO}$  J=3–2 at 345.796 GHz and  $\text{HCO}^+$  J=4–3 at 356.734 GHz, mapping a region of  $2' \times 2'$  centered at RA =  $18^{\text{h}}22^{\text{m}}11.39^{\text{s}}$ , dec.= $-14^{\circ}35'24.81''$  (J2000). We also observed  $^{13}\text{CO}$  J=3–2 at 330.588 GHz and CS J=7–6 at 342.883 GHz towards the same region. The mapping grid spacing was  $20''$  in both cases and the integration time was 20 sec ( $^{12}\text{CO}$  and  $\text{HCO}^+$ ) and 40 sec ( $^{13}\text{CO}$  and CS) per pointing. All the observations were performed in position switching mode. We verified that the off position was free of emission. We used the XF digital spectrometer with a bandwidth and spectral resolution set to 128 MHz and 125 kHz, respectively. The velocity resolution was  $0.11\ \text{kms}^{-1}$  and the half-power beamwidth

(HPBW) was about  $22''$  for all observed molecular lines. The system temperature varied from  $T_{\text{sys}} = 150$  to  $200$  K. The main beam efficiency was  $\eta_{\text{mb}} \sim 0.65$ . All the spectra were Hanning smoothed to improve the signal-to-noise ratio. The baseline fitting was carried out using second order polynomials for the  $^{12}\text{CO}$  and  $^{13}\text{CO}$  transitions and third order polynomials for the  $\text{HCO}^+$  and CS transitions. The polynomials were the same for all spectra of the map at a given transition. The resulting rms noise of the observations was about  $0.2$  K for  $^{13}\text{CO}$  J=3–2 and CS J=7–6, and about  $0.4$  K for  $^{12}\text{CO}$  J=3–2 and  $\text{HCO}^+$  J=4–3 transitions.

## 2.2. Radio continuum observations

The radio continuum observations towards the bright-rimmed cloud were performed in a single pointing with the Karl G. Jansky Very Large Array (JVLA) in its C configuration, on 2012 February 7 and 12 (project ID:12A-020) for a total of 70 minutes on-source integration time. We used the wideband 4–8 GHz receiver system centered at 4.7 and 7.4 GHz, which consists in 16 spectral windows with a bandwidth of 128 MHz each, spread into 64 channels. Data processing was carried out using the CASA and Miriad software packages, following standard procedures. The source J1331+3030 was used for primary flux density and bandpass calibration, while phases were calibrated with J1820-2528. For the scope of this paper we only reconstructed an image centered at 5 GHz with a bandwidth of 768 MHz using the task MAXEN in MIRIAD, which performs a maximum entropy deconvolution algorithm on a cube. The resulting synthesised beam has a size of  $7''.5 \times 5''.4$ , and the rms noise of the final map is  $0.016$  mJy/beam.

The observations are complemented with  $\text{H}\alpha$ , near- and mid-IR data extracted from public databases and catalogs, which are described in the corresponding sections.

## 3. Results and Analysis

### 3.1. The molecular gas

Figure 2(left-column) shows the  $^{12}\text{CO}$  J=3–2 (a),  $^{13}\text{CO}$  J=3–2 (b),  $\text{HCO}^+$  J=4–3 (c), and CS J=7–6 (d) spectra obtained towards the  $2' \times 2'$  analyzed region (white box in Fig. 1). The corresponding profiles towards the positions (0, 0) are also shown in the right-column of the figure. The  $^{12}\text{CO}$  J=3–2 profile towards the (0, 0) offset exhibits a quintuple peak structure with components centered at about 27, 31, 38, 42, and  $45 \text{ km s}^{-1}$ . In particular, the velocity component centered at about  $38 \text{ km s}^{-1}$ , which is detected towards the central region, is most intense at this position, while the component centered at about  $45 \text{ km s}^{-1}$ , whose velocity coincides with the systemic velocity of the molecular cloud related to Sh2-48 is most intense at the position  $(-40, +40)$ . The  $^{13}\text{CO}$  J=3–2 spectrum at the (0, 0) position exhibits a behavior similar to that of  $^{12}\text{CO}$  J=3–2 with the same five velocity components centered at 27, 31, 38, 42, and  $45 \text{ km s}^{-1}$ . As in the case of the  $^{12}\text{CO}$  J=3–2 emission, the component centered at  $38 \text{ km s}^{-1}$  is most intense at this position and the intensity maximum of the component at  $45 \text{ km s}^{-1}$  is at the  $(-40, +40)$  offset. The  $\text{HCO}^+$  J=4–3 line has a single velocity component above  $3\sigma$  centered at  $38.4 \text{ km s}^{-1}$  towards the (0, 0) position. Finally, the

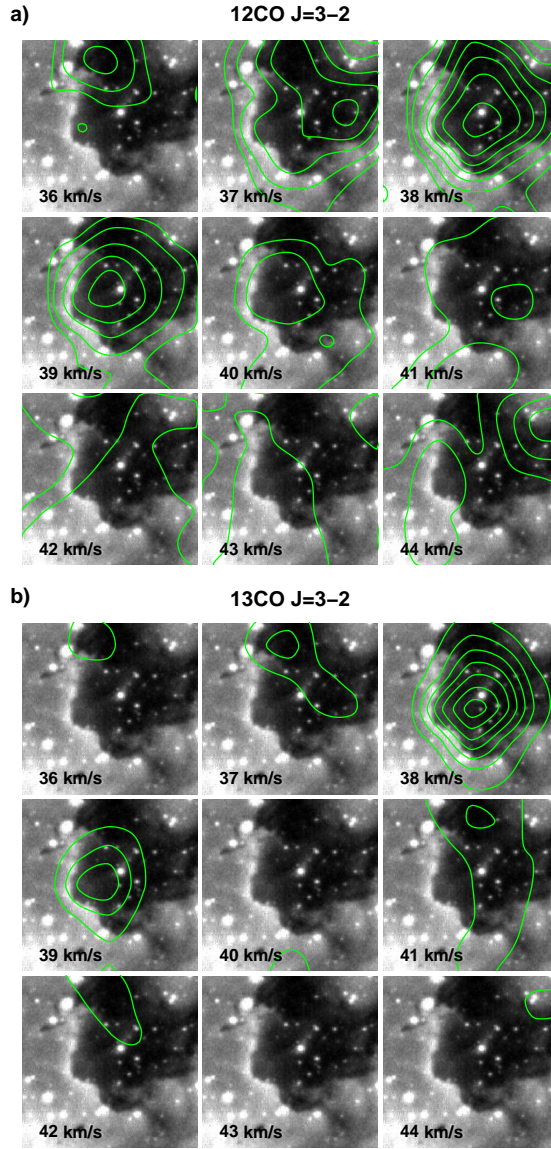


**Fig. 3.** Velocity channel maps of the  $^{12}\text{CO}$  J=3–2 (a) and  $^{13}\text{CO}$  J=3–2 (b) emission from 35 to 44  $\text{km s}^{-1}$  integrated every 1  $\text{km s}^{-1}$  (green contours) superimposed onto the  $\text{H}_\alpha$  emission of the BRC. The given velocities correspond to the higher velocity of each interval. Contours are plotted above the  $5\sigma$  of the rms noise level.

CS J=7–6 spectrum at the (0, 0) offset also shows a single velocity component centered at about 38.5  $\text{km s}^{-1}$  above  $3\sigma$  of the rms noise level. The detection of this molecular transition reveals the presence of warm and dense gas mapping the dense core of the cloud. The velocity component related to the BRC is 6  $\text{km s}^{-1}$  blue-shifted respect to the systemic velocity of the parental molecular cloud in which it is embedded. This fact suggests that the molecular clump has probably been pushed forward by the O star and currently it is moving in our direction with respect to the centre of the complex. This result is in agreement with the predictions of the works of Pittard et al. (2009) and Mizuta et al. (2006), which based on simulations of radiative and shock destruction of clouds, have shown that the head of a pillar in a molecular cloud exposed to the action of a neighboring massive star, is accelerated outward or evaporated. As such, the position of the pillar head is offset from the initial cloud position.



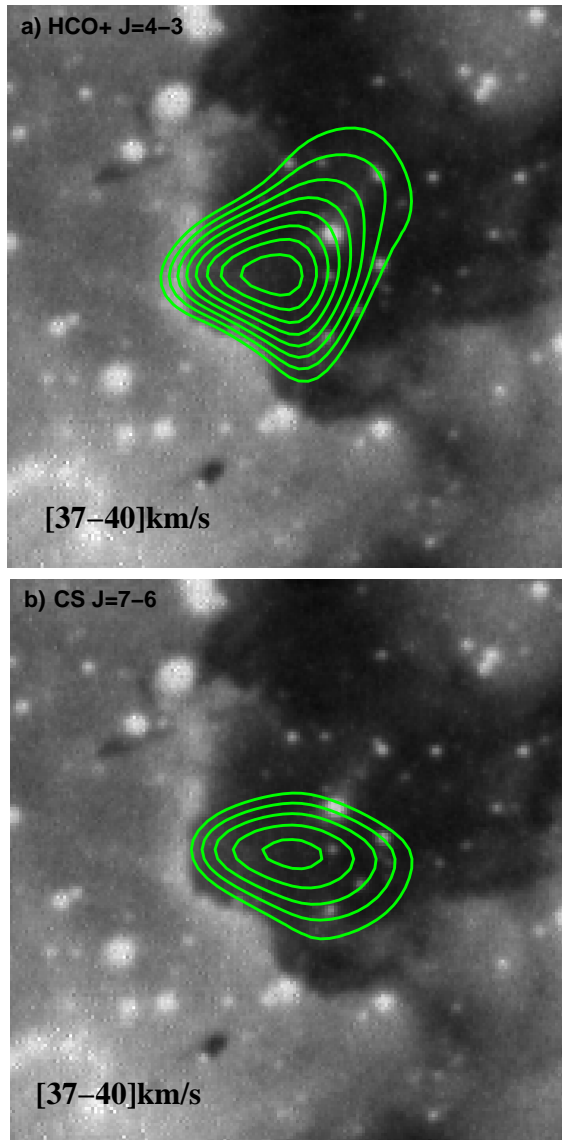


**Fig. 4.** a) Emission distribution of the  $\text{HCO}^+$   $J=4-3$  transition integrated between 37 and 40  $\text{km s}^{-1}$  (green contours) superimposed onto the  $\text{H}_\alpha$  emission of the BRC. Contours levels go from 0.8 to 2.2  $\text{K km s}^{-1}$  in steps of 0.2  $\text{K km s}^{-1}$ . b) Emission distribution of the CS  $J=7-6$  transition integrated between 37 and 40  $\text{km s}^{-1}$  (green contours) superimposed onto the  $\text{H}_\alpha$  emission of the BRC. Contours levels are at 0.3, 0.4, 0.5, 0.6, and 0.7  $\text{K km s}^{-1}$ .

In Figure 3 we show the velocity channel maps of the  $^{12}\text{CO}$   $J=3-2$  (a) and the  $^{13}\text{CO}$   $J=3-2$  (b) emission distributions from 35 to 44  $\text{km s}^{-1}$ , integrated every 1  $\text{km s}^{-1}$  (green contours) superimposed onto the  $\text{H}_\alpha$  image of the BRC. As can be seen from this figure, the  $^{12}\text{CO}$   $J=3-2$  emission distribution is well correlated with the BRC between 36 and 40  $\text{km s}^{-1}$  and the  $^{13}\text{CO}$   $J=3-2$  emission around 38  $\text{km s}^{-1}$  exhibits an excellent morphological correlation with the BRC as seen in the optical image.

Figure 4 shows the  $\text{HCO}^+$   $J=4-3$  (a) and the CS  $J=7-6$  (b) emission distributions above  $3\sigma$  of the rms noise level integrated between 37 and 40  $\text{km s}^{-1}$  (green contours) superimposed onto the  $\text{H}_\alpha$  image of the BRC. From this figure it can be seen the good morphological correlation between the  $\text{HCO}^+$   $J=4-3$  emission distribution with the curved  $\text{H}_\alpha$  features of the BRC. Besides, the intensity gradient seems to be steeper in the direction of the ionizing star, suggesting a possible compression



**Table 1.** Emission peaks parameters derived from a Gaussian fitting for the four molecular transitions on the position (0, 0).

| Transition             | $V_{LSR}$ [kms <sup>-1</sup> ] | $T_{mb}$ [K] | $\Delta v$ [kms <sup>-1</sup> ] |
|------------------------|--------------------------------|--------------|---------------------------------|
| CS J=7–6               | 38.5±0.9                       | 0.6±0.2      | 1.8±0.6                         |
| HCO <sup>+</sup> J=4–3 | 38.4±0.4                       | 1.5±0.2      | 2.0±0.5                         |
| <sup>13</sup> CO J=3–2 | 26.9 ± 0.6                     | 0.7 ± 0.2    | 1.5 ± 0.6                       |
|                        | 30.7 ± 0.4                     | 0.8 ± 0.3    | 1.8 ± 0.6                       |
|                        | 38.1 ± 0.4                     | 8.1 ± 0.3    | 1.9 ± 0.7                       |
|                        | 41.8 ± 0.6                     | 1.3 ± 0.4    | 1.5 ± 0.4                       |
|                        | 44.6 ± 0.5                     | 0.6 ± 0.4    | 3.1 ± 0.4                       |
| <sup>12</sup> CO J=3–2 | 26.9±0.1                       | 2.2±1.1      | 3.6±0.4                         |
|                        | 30.8±0.2                       | 2.9±0.8      | 3.6±0.6                         |
|                        | 37.9±0.6                       | 14.1±0.7     | 2.9±0.5                         |
|                        | 42.2±0.4                       | 4.2±0.2      | 2.8±0.4                         |
|                        | 45.1±0.5                       | 1.2±0.2      | 3.3±0.4                         |

on the molecular gas. The molecular clump detected at the CS J=7–6 transition is slightly set back from the bright rim with respect to the direction of the ionizing star. The maximum of the emission of both lines, HCO<sup>+</sup> J=4–3 and CS J=7–6, are positionally coincident.

Table 1 lists the emission peaks parameters derived from a Gaussian fitting for the four molecular transitions on the position (0, 0).  $V_{LSR}$  represents the central velocity referred to the Local Standard of Rest,  $T_{mb}$  the peak brightness temperature, and  $\Delta v$  the line FWHM. Errors are formal  $1\sigma$  value for the model of Gaussian line shape. All velocities are in the local standard of rest.

### 3.2. Column density and mass estimates of the molecular clump

Assuming LTE conditions we estimate the <sup>13</sup>CO J=3–2 opacity,  $\tau_{13}$ , based on the following equation:

$$\tau_{13} = -\ln \left( 1 - \frac{T_{peak}({}^{13}\text{CO})}{T_{peak}({}^{12}\text{CO})} \right) \quad (1)$$

where the  $T_{peak}$  at 38 kms<sup>-1</sup> was measured at the position (0, 0) for both transitions. We obtain  $\tau_{13} \sim 0.8$ , which suggests that the <sup>13</sup>CO J=3–2 line can be considered optically thin in this molecular condensation.

The excitation temperature,  $T_{ex}$ , of the <sup>13</sup>CO J=3–2 line is estimated from:

$$T_{peak}({}^{13}\text{CO}) = \frac{h\nu}{k} \left( \frac{1}{e^{h\nu/kT_{ex}} - 1} - \frac{1}{e^{h\nu/kT_{BG}} - 1} \right) \times (1 - e^{-\tau_{13}}) \quad (2)$$

where for this transition  $h\nu/k = 15.87$ . Assuming  $T_{BG} = 2.7$  K, and considering the  $T_{peak}({}^{13}\text{CO}) = 8$  K, we derive a  $T_{ex} \sim 21$  K for this line. This value is significantly higher than would be expected for a starless clump ( $T \leq 10$  K; Shinnaga et al. 2004), evidencing that the molecular clump has an

internal heating mechanism. Then, we derive the  $^{13}\text{CO}$  column density from (see e.g. Buckle et al. 2010):

$$N(^{13}\text{CO}) = 8.28 \times 10^{13} e^{\frac{15.87}{T_{ex}}} \frac{T_{ex} + 0.88}{1 - \exp(-\frac{15.87}{T_{ex}})} \int \tau_{13} dv \quad (3)$$

where, taking into account that  $^{13}\text{CO}$  J=3–2 transition can be considered optically thin, we use the approximation:

$$\int \tau dv = \frac{1}{J(T_{ex}) - J(T_{BG})} \int T_{mb} dv \quad (4)$$

with

$$J(T) = \frac{h\nu/k}{\exp(\frac{h\nu}{kT}) - 1}. \quad (5)$$

From the estimated  $N(^{13}\text{CO}) \sim 8 \times 10^{15} \text{ cm}^{-2}$ , and assuming the  $[\text{H}_2]/[^{13}\text{CO}] = 77 \times 10^4$  ratio (Wilson & Rood 1994), we derive an  $\text{H}_2$  column density,  $N(\text{H}_2) \sim 6 \times 10^{21} \text{ cm}^{-2}$ . Using the relation  $M = \mu m_H d^2 \Omega N(\text{H}_2)$ , where  $\mu$  is the mean molecular weight per  $\text{H}_2$  molecule ( $\mu \sim 2.72$ ),  $m_H$  the hydrogen atomic mass,  $d$  the distance, and  $\Omega$  the solid angle subtended by the structure, then the total mass of the clump turns out to be  $M \sim 180 M_\odot$  and the volume density,  $n(\text{H}_2) \sim 3 \times 10^3 \text{ cm}^{-3}$ . The errors in these estimates are about 30% and 40%, respectively.

We also independently calculate the mass and the volume density of the clump based on the associated dust continuum emission. In particular, we use the integrated flux of the continuum emission at 1.1 mm as obtained from The Bolocam Galactic Plane Survey II Catalog (BGPS II; Rosolowsky et al. 2010). Following Beuther et al. (2002) and Hildebrand (1983), and considering the flux estimated with the aperture of  $80''$ , to be comparable in size with the BRC, we calculate the mass of the clump in solar masses from:

$$M_{gas} = \frac{1.3 \times 10^{-3}}{J_\nu(T_{dust})} \frac{a}{0.1 \mu\text{m}} \frac{\rho}{3 \text{ g cm}^{-3}} \frac{R}{100 \text{ Jy}} \left( \frac{d}{\text{kpc}} \right)^2 \left( \frac{\nu}{2.4 \text{ THz}} \right)^{-3-\beta}$$

where  $J_\nu(T_{dust}) = [\exp(h\nu/kT_{dust}) - 1]^{-1}$  and  $a, \rho, R$ , and  $\beta$  are the grain size, grain mass density, gas-to-dust ratio, and grain emissivity index for which we adopt the values of  $0.1 \mu\text{m}$ ,  $3 \text{ g cm}^{-3}$ , 100, and 2, respectively (Hunter 1997, Hunter et al. 2000, and Molinari et al. 2000). Assuming a dust temperature of 20 K and considering the integrated flux intensity  $S_{80} = 0.285 \text{ Jy}$  at 1 mm (Rosolowsky et al. 2010), we obtain  $M_{gas} \sim 260 M_\odot$  and a volume density,  $n(\text{H}_2) \sim 3 \times 10^3 \text{ cm}^{-3}$ , in good agreement with those values derived from the LTE calculations using the  $^{12}\text{CO}$  J=3–2 and  $^{13}\text{CO}$  J=3–2 transitions.

### 3.3. The ionized boundary layer associated with the BRC

Figure 5 shows the new JVLA radio continuum emission at 5 GHz (green contours) superimposed onto the  $H_\alpha$  image of the BRC. At first glance, it can be appreciate the radio continuum emission related to Sh2-48, extending over most of the studied region. A noticeable radio feature is the arc-like radio filament that perfectly matches the optical emission of the bright rim related to the curved feature A. This positional and morphological correlation suggests that this radio continuum emission arises from the ionized gas located in the illuminated border of the molecular clump. Thus, the radio continuum emission allow us to estimate the ionizing photon flux impinging upon the illuminated face of the BRC and the electron density of the ionized boundary layer. We estimate the radio continuum flux density of the arc-like radio filament at 5 GHz in  $2.3 \times 10^{-4}$  Jy.

Assuming that all of the ionizing photon flux is absorbed within the IBL, we determine the photon flux,  $\Phi$ , and the electron density,  $n_e$ , using the equations detailed by Lefloch et al. (1997) and modified by Thompson et al. (2004):

$$\Phi = 1.24 \times 10^{10} S_\nu T_e^{0.35} \nu^{0.1} \theta^{-2} [\text{cm}^{-2} \text{s}^{-1}] \quad (6)$$

$$n_e = 122.21 \times \left( \frac{S_\nu T_e^{0.35} \nu^{0.1}}{\eta R \theta^2} \right)^{1/2} [\text{cm}^{-3}] \quad (7)$$

where  $S_\nu$  is the integrated flux density in mJy,  $\nu$  is the frequency in GHz,  $\theta$  is the angular diameter over which the flux density is integrated in arc-seconds,  $\eta R$  is the shell thickness in pc, and  $T_e$  is the electron temperature in K. Assuming an average electron temperature of about  $10^4$  K and an  $\eta = 0.2$  (Bertoldi 1989), and considering an effective  $\theta$  of about  $12''$  and a clump radius  $R \sim 0.6'$  (about 0.67 pc at the distance of 3.8 kpc), we derive the photon flux and electron density values of  $\Phi \sim 5.8 \times 10^8 \text{cm}^{-2} \text{s}^{-1}$  and  $n_e \sim 73 \text{cm}^{-3}$ , respectively. The main sources of error in the electron density estimate come from the assumption on  $\eta$  and from the uncertainty in the distance, which combined give an error of about 40%.

The mean electron density value obtained for the IBL is almost a factor three greater than the critical value of  $n_e \sim 25 \text{cm}^{-3}$ , above which an IBL is able to develop around a molecular clump (Lefloch & Lazareff 1994). This fact reinforces the hypothesis that the clump is being photoionized by the nearby O9.5V star. However, it is not clear to what extent the ionization has influenced the evolution of the cloud, and what role, if any, has played in triggering star formation.

Finally, we also calculate the predicted ionized flux,  $\Phi_{pred}$ , of the IBL considering a Lyman photon flux of about  $1.8 \times 10^{48} \text{ph s}^{-1}$  (Schaerer & de Koter 1997) for the ionizing star BD-14 5014 which is located at least 3 pc away from the clump. The predicted ionized photon flux,  $\Phi_{pred} \sim 16.7 \times 10^8 \text{cm}^{-2} \text{s}^{-1}$  is three times greater than the value estimated from the radio continuum

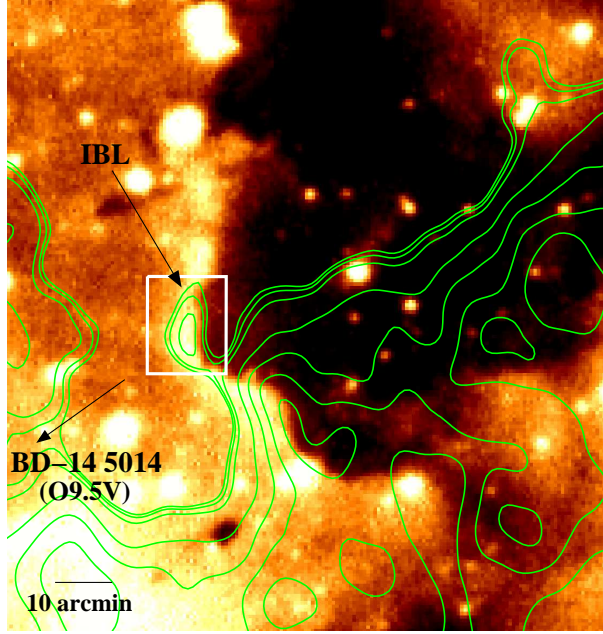


**Fig. 5.**  $H_\alpha$  image of the BRC. The green contours represent the radio continuum emission at 5 GHz. Contours levels are at 0.7 (about  $4\sigma$  above the rms noise level), 0.9, 1, 2, 3, 4, and  $5 \times 10^{-4}$  Jy/beam. The white box indicates the IBL region associated with the protrusion A.

observations, which is not surprising given that the former is a strict upper limit due to projection effects and dust absorption.

## 4. Discussion

### 4.1. Testing the RDI mechanism through a pressure balance analysis

To evaluate the pressure balance between the ionized gas of the IBL and the neutral gas of the molecular cloud we use the results of Sections 3.2 and 3.3. The analysis of the balance between the external and internal pressures,  $P_{ext}$  and  $P_{int}$ , respectively, gives a good piece of information about the influence that the ionization front has had in the evolution of the BRC. Following Thompson et al. (2004) the pressures are defined as:

$$P_{int} \simeq \sigma^2 \rho_{int} \quad (8)$$

$$P_{ext} = 2\rho_{ext}c^2 \quad (9)$$

where  $\sigma^2$  is the square of the velocity dispersion, defined as  $\sigma^2 = \Delta v^2 / (8 \ln 2)$ , with  $\Delta v$  the line width of the  $^{13}\text{CO}$  J=3–2 line taken from the profile at the (0, 0) offset,  $\rho_{int}$  is the clump density,  $\rho_{ext}$  the ionized gas density, and  $c \sim 11.4 \text{ km s}^{-1}$  (e.g. Urquhart et al. 2006) a typical sound speed for these regions. To estimate the ionized gas pressure for the IBL we use the electron density calculated in Sect. 3.3, obtaining  $P_{ext}/k_B \sim 23 \times 10^5 \text{ cm}^{-3} \text{ K}$ , which is among the lowest values

estimated in similar regions (see e.g. Morgan et al. 2004). To estimate the internal pressure of the molecular clump, we use the  $\text{H}_2$  volume density,  $n(\text{H}_2)$ , calculated in Sect. 3.2, yielding a  $P_{\text{int}}/k_B \sim 5 \times 10^5 \text{ cm}^{-3} \text{ K}$ .

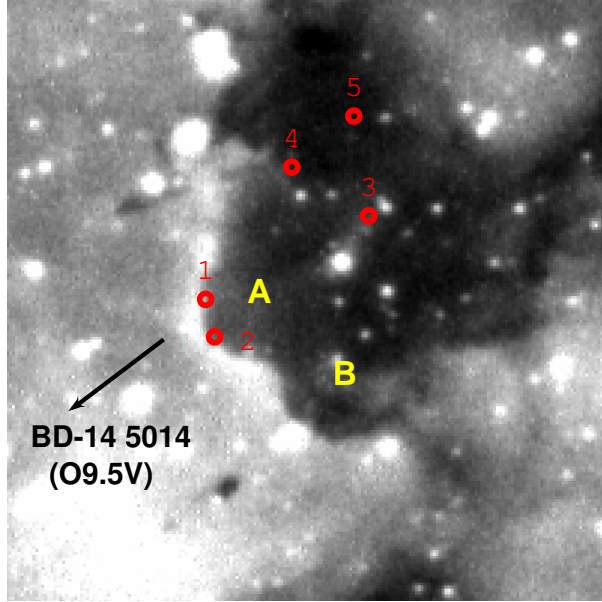
The comparison between both pressures reveals that the clump is under pressure by a factor four with respect to its IBL, suggesting that the shocks are currently being driven into the surface layers. In this way, the BRC could be in a pre-pressure balance state, where the H II region has only recently begun to affect the molecular gas and shocks have not propagated very far into the clump. Thus, it is likely that the molecular clump predate the arrival of the ionization front.

#### 4.2. Young stellar object population

Given the result of previous section, any young stellar object (YSO) triggered via the radiation-driven implosion mechanism should be placed at the illuminated border of the BRC. In this section we look for YSO candidates associated with the molecular condensation. YSOs use to be classified based on their evolutive stage: class I are the youngest sources which are still embedded in dense envelopes of gas and dust, and class II are those sources whose emission is mainly originated in the accretion disk surrounding the central protostar. In both cases, a YSO will exhibit an infrared excess which is mainly due to the presence of the envelope and/or the disk of dust around the central object, but not attributed to the scattering and absorption of the interstellar medium along the line of sight. In other words, YSOs are intrinsically red sources. Robitaille et al. (2008) defined an infrared color criterion to identify intrinsically red sources based on *Spitzer* data. They must satisfy the condition  $[4.5] - [8.0] \geq 1$ , where  $[4.5]$  and  $[8.0]$  are the magnitudes in the 4.5 and 8.0  $\mu\text{m}$  bands, respectively. Following this criterion we find five intrinsically red sources towards the region of the BRC and its surroundings. In Table 2 we report the magnitudes of the intrinsically red sources in the *Spitzer*-IRAC bands (Col. 3-6), specifying the GLIMPSE designation (Col. 2) and the Allen et al. (2004) classification (Col. 7), and in Figure 6 we show their location. Sources #1 and #2 are located at the border of the bright rim labeled A, they are spatially separated from the other three embedded sources, and are young class I YSOs. All these characteristics support the possibility that the RDI processes have triggered their formation. However, we can not discard that both YSOs have been formed previously by other mechanism and now are being unveiled by the advancing ionization front. Given that the BRC would be located in the near part of the molecular complex, due to projection effects we can not rule out that the YSOs #1 and #2 are currently detached from the clump. In any case, if the newly born stars are massive, their feedback may ultimately destroy their natal molecular cloud shutting off star formation or may simultaneously trigger the birth of new generations of stars, as in the scenario of progressive star formation in the Carina nebula described by Smith et al. (2010). Depending on how massive the recently formed stars are, they will affect more or less the local environment of the BRC. Future works tending to characterize these sources will be relevant to disentangle such effects.

**Table 2.** Mid-IR magnitudes and Allen et al. (2004) classification of the point sources satisfying the condition  $[4.5] - [8.0] \geq 1$  towards the BRC.

| Source | GLIMPSE Desig.    | 3.6 $\mu\text{m}$<br>(mag) | 4.5 $\mu\text{m}$<br>(mag) | 5.8 $\mu\text{m}$<br>(mag) | 8.0 $\mu\text{m}$<br>(mag) | Class |
|--------|-------------------|----------------------------|----------------------------|----------------------------|----------------------------|-------|
| YSO 1  | G016.6534-00.3062 | 13.140                     | 12.744                     | 10.871                     | 9.663                      | I     |
| YSO 2  | G016.6511-00.3068 | 11.603                     | 11.368                     | 10.880                     | 10.366                     | I     |
| YSO 3  | G016.6532-00.2948 | 12.798                     | 12.911                     | 12.187                     | 11.314                     | I     |
| YSO 4  | G016.6582-00.2976 | 11.714                     | 11.569                     | 10.882                     | 9.961                      | II    |
| YSO 5  | G016.6592-00.2926 | 14.317                     | 13.850                     | -                          | 9.017                      | -     |

**Fig. 6.** Spatial distribution of the YSO candidates towards the BRC. Their positions are indicated with the red circles. The black arrow shows the direction of the ionizing star.

Concerning the YSOs #3, #4, and #5, the fact that the shocks induced by the H II region Sh2-48 are being driven into the external layer of the BRC (see Section 4.1), it is unlikely that these sources have been triggered via the radiation-driven implosion mechanism.

## 5. Summary

We present new molecular observations in the  $^{12}\text{CO}$  J=3–2,  $^{13}\text{CO}$  J=3–2,  $\text{HCO}^+$  J=4–3, and CS J=7–6 lines using the Atacama Submillimeter Telescope Experiment (ASTE), and radio continuum observations at 5 GHz using the Karl Jansky VLA instrument, towards a new bright-rimmed cloud (BRC) located near the border of the H II region Sh2-48.

The molecular observations in the different lines reveal the presence of a relatively dense clump in very good spatial correspondence with the BRC as observed in the  $\text{H}_\alpha$  emission.

The high angular resolution and sensitivity radio continuum data have revealed the presence of an arc-like radio filament in excellent correspondence with the brightest border of the optical emission of the BRC, highly suggestive to be the associated ionized boundary layer (IBL). We derive an electron density for the IBL of about  $73 \text{ cm}^{-3}$ . This value is three times higher than the critical density above which an IBL can form and be maintained. The location and morphology of

the radio filament, together with the estimate of the electron density support the hypothesis that the BRC is being photoionized by the exciting star of Sh2-48. From the CO and radio continuum data we estimate the pressure balance between the IBL and the molecular gas, finding that the BRC is likely to be in a pre-pressure state.

We have also studied the star formation activity in the region. We find five YSO candidates embedded in the BRC. Two of them are located in projection towards the illuminated border of the BRC and are most probably formed via the RDI mechanism.

## Acknowledgments

We wish to thank the referee, Dr. Gahm, whose constructive criticism has helped make this a better paper. M.O., S.P., E.G., and G.D. are members of the *Carrera del Investigador Científico* of CONICET, Argentina. This work was partially supported by Argentina grants awarded by Universidad de Buenos Aires (UBACyT 01/W011), CONICET and ANPCYT. M.R. wishes to acknowledge support from FONDECYT (CHILE) grant No108033. She is supported by the Chilean Center for Astrophysics FONDAF No. 15010003. The ASTE project is driven by Nobeyama Radio Observatory (NRO), a branch of National Astronomical Observatory of Japan (NAOJ), in collaboration with University of Chile, and Japanese institutes including University of Tokyo, Nagoya University, Osaka Prefecture University, Ibaraki University, Hokkaido University and Joetsu University of Education.

## References

- Allen, L. E., Calvet, N., D'Alessio, P., et al. 2004, *ApJS*, 154, 363
- Anderson, L. D., Bania, T. M., Jackson, J. M., et al. 2009, *ApJS*, 181, 255
- Avedisova, V. S. & Kondratenko, G. I. 1984, *Nauchnye Informatsii*, 56, 59
- Bertoldi, F. 1989, *ApJ*, 346, 735
- Bertoldi, F. & McKee, C. F. 1990, *ApJ*, 354, 529
- Beuther, H., Schilke, P., Menten, K. M., et al. 2002, *ApJ*, 566, 945
- Blitz, L., Fich, M., & Stark, A. A. 1982, *ApJS*, 49, 183
- Buckle, J. V., Curtis, E. I., Roberts, J. F., et al. 2010, *MNRAS*, 401, 204
- Churchwell, E., Povich, M. S., Allen, D., et al. 2006, *ApJ*, 649, 759
- Crampton, D., Georgelin, Y. M., & Georgelin, Y. P. 1978, *A&A*, 66, 1
- Deharveng, L., Schuller, F., Anderson, L. D., et al. 2010, *A&A*, 523, A6
- Ezawa, H., Kawabe, R., Kohno, K., & Yamamoto, S. 2004, in *Society of Photo-Optical Instrumentation Engineers (SPIE) Conference Series*, Vol. 5489, *Society of Photo-Optical Instrumentation Engineers (SPIE) Conference Series*, ed. J. M. Oschmann Jr., 763–772
- Hildebrand, R. H. 1983, *QJRAS*, 24, 267
- Hunter, T. R. 1997, PhD thesis, Smithsonian Astrophysical Observatory, 60 Garden St. MS-78, Cambridge, MA 02178, USA
- Hunter, T. R., Churchwell, E., Watson, C., et al. 2000, *AJ*, 119, 2711
- Lefloch, B. & Lazareff, B. 1994, *A&A*, 289, 559
- Lefloch, B., Lazareff, B., & Castets, A. 1997, *A&A*, 324, 249
- Lockman, F. J. 1989, *ApJS*, 71, 469



- Megeath, S. T. & Wilson, T. L. 1997, *AJ*, 114, 1106
- Mizuta, A., Kane, J. O., Pound, M. W., et al. 2006, *ApJ*, 647, 1151
- Molinari, S., Brand, J., Cesaroni, R., & Palla, F. 2000, *A&A*, 355, 617
- Morgan, L. K., Thompson, M. A., Urquhart, J. S., White, G. J., & Miao, J. 2004, *A&A*, 426, 535
- Morgan, L. K., Thompson, M. A., Urquhart, J. S., & White, G. J. 2008, *A&A*, 477, 557
- Ogura, K., Sugitani, K., & Pickles, A. 2002, *AJ*, 123, 2597
- Pittard, J. M., Falle, S. A. E. G., Hartquist, T. W., & Dyson, J. E. 2009, *MNRAS*, 394, 1351
- Reipurth, B. 1983, *A&A*, 117, 183
- Robitaille, T. P., Meade, M. R., Babler, B. L., et al. 2008, *AJ*, 136, 2413
- Rosolowsky, E., Dunham, M. K., Ginsburg, A., et al. 2010, *ApJS*, 188, 123
- Sandford, II, M. T., Whitaker, R. W., & Klein, R. I. 1982, *ApJ*, 260, 183
- Schaerer, D. & de Koter, A. 1997, *A&A*, 322, 598
- Sharpless, S. 1959, *ApJS*, 4, 257
- Shinnaga, H., Ohashi, N., Lee, S.-W., & Moriarty-Schieven, G. H. 2004, *ApJ*, 601, 962
- Smith, N., Povich, M. S., Whitney, B. A., et al. 2010, *MNRAS*, 406, 952
- Sugitani, K., Fukui, Y., & Ogura, K. 1991, *ApJS*, 77, 59
- Sugitani, K. & Ogura, K. 1994, *ApJS*, 92, 163
- Sugitani, K., Tamura, M., & Ogura, K. 1995, *ApJ*, 455, L39
- Sugitani, K., Matsuo, H., Nakano, M., Tamura, M., & Ogura, K. 2000, *AJ*, 119, 323
- Thompson, M. A., Urquhart, J. S., & White, G. J. 2004, *A&A*, 415, 627
- Urquhart, J. S., Thompson, M. A., Morgan, L. K., & White, G. J. 2006, *A&A*, 450, 625
- Urquhart, J. S., Morgan, L. K., & Thompson, M. A. 2009, *A&A*, 497, 789
- Vijapurkar, J. & Drilling, J. S. 1993, *ApJS*, 89, 293
- Vogt, N. & Moffat, A. F. J. 1975, *A&A*, 45, 405
- Wilson, T. L. & Rood, R. 1994, *ARA&A*, 32, 191
- Wootten, A., Sargent, A., Knapp, G., & Huggins, P. J. 1983, *ApJ*, 269, 147

## List of Objects